Heliyon 10 (2024) e34381

Contents lists available at ScienceDirect

Heliyon

journal homepage: www.cell.com/heliyon

Research article

Ferroptosis-related alternative splicing signatures as potential biomarkers for predicting prognosis and therapy response in gastric cancer

Gang Long [a,1], Zhiyong Li [b,1], Yue Gao [a], Xu Zhang [a], Xiyang Cheng [a], Irankunda Eric Daniel [a], Lisha Zhang [a], Dawei Wang [a], Zhengtian Li [a,*]

[a] Department of General Surgery, The First Affiliated Hospital of Harbin Medical University, No.23 Post Street, Nangang district, Harbin, 150007, China

[b] Department of General Surgery, Peking University People's Hospital, Beijing, 100044, China

ARTICLE INFO

Keywords:
Ferroptosis
Gastric cancer
Prognosis
Alternative splicing
Tumor microenvironment

ABSTRACT

Ferroptosis is linked to various tumor biological traits, and alternative splicing (AS), a crucial step in mRNA processing, plays a role in the post-transcriptional regulation of ferroptosis-related genes (FRGs). A least absolute shrinkage and selection operator (LASSO) penalized Cox regression analysis was utilized to build a prognostic signature based on 12 AS events ($p < 0.05$), which was validated in gastric cancer (GC) patients. The high-risk group ($n = 203$) showed enrichment in cancer and metastasis pathways ($p < 0.05$). Significant differences existed between the high- and low-risk groups in terms of tumor microenvironment (TME) cell infiltration and immune activities ($p < 0.05$). The low-risk group ($n = 203$) was characterized by immune activation and improved prognosis ($p < 0.001$). Additionally, targeted treatment and immunotherapy were more likely to benefit the low-risk group ($p < 0.05$). Correlation analysis was performed to detect related splicing factors (SF) (Cor>0.4, FDR<0.05). Furthermore, our functional assay results suggested that high SF3A2 expression might increase ferroptosis resistance and promote cell proliferation. In conclusion, the FRAs model we built has an advantage in predicting GC prognosis. The model's demonstration of variations in the immune microenvironment and drug response could potentially inform decisions regarding treatment strategies.

1. Introduction

GC is the third leading cause of death among digestive tumors and the fifth leading cause of death globally [1,2]. Although surgery is the most effective treatment for GC, individuals with advanced GC have a median survival duration of only approximately one year [3]. Consequently, there is a critical need for new biomarkers and molecular targets to improve therapeutic strategies and prognosis for patients with GC. The characteristics of FRGs are effective in distinguishing GC prognosis [4,5]. Previous studies have primarily focused on coding and noncoding RNAs associated with ferroptosis; however, few have examined the characteristics of FRG transcripts. These enriched RNAs under AS parameters could more comprehensively characterize the differential genes in GC patients.

* Corresponding author.
E-mail address: 601059@hrbmu.edu.cn (Z. Li).

[1] These authors have contributed equally to this work and share first authorship.

https://doi.org/10.1016/j.heliyon.2024.e34381
Received 21 September 2023; Received in revised form 4 July 2024; Accepted 9 July 2024
Available online 10 July 2024

Ferroptosis is a type of peroxidation-induced cell death dependent on abundant and readily accessible cytosolic iron. Morphologically, biochemically, and genetically, ferroptosis differs with apoptosis, necrosis, and autophagy [6]. Significant accumulation of lipid reactive oxygen species (ROS) and iron-dependent activation by erastin, RSL3, and regulatory chemicals characterize this process [7]. It has been established that the processes controlling ferroptosis are strongly linked to cysteine and glutathione metabolism, as well as the ability of phospholipid peroxidase 4 (GPX4) to inhibit the formation of lipid peroxide [8]. Ferroptosis may play a physiological role in tumor suppression and immunology. Induction of ferroptosis has been conclusively proven to be a viable cancer treatment method [9]. Recent research has demonstrated that ferroptosis dysfunction plays a significant role in the progression of GC [10–12]. Compared to other types of tumors, the effects of ferroptosis in GC are well studied. Previous research has identified functional genes that partially regulate ferroptosis or serve as ferroptosis indicators in various diseases [13]. FerrDb, the first database to collect ferroptosis regulators and indicators, contains 253 regulators and analyzes the associations of ferroptosis with disease [14]. Therefore, developing more precise FRG biomarkers and analyzing FRG signatures, as well as the investigation of prognosis-related biomarkers based on biological and molecular mechanisms in GC, are essential for the development of precise, individualized treatment regimens.

More than 95 % of human genes undergo various degrees of AS [15]. Consequently, AS significantly expands the structure and function of the human proteome [16]. AS is regulated by RNA-binding proteins (RBPs) known as SF [17]. Serine/arginine (SR) residue-rich splicing regulatory proteins (also known as SR proteins) and heterogeneous ribonucleoproteins (hRNPs) are the two most prevalent SFs [18]. Substantial evidence indicates that aberrant splicing events contribute to the development of specific cancers [19]. In one study, more than 8000 samples from 32 distinct malignancies were evaluated, revealing thousands of splice isoforms in tumor tissue but not in noncancerous tissue [20]. AS events have been shown to be predictive for a range of cancer types [21]. MAP2K7exon2-driven dedifferentiation of GC cells in the MBNL1-low subpopulation is one example. MBNL1 downregulation in gastric cancer is predictive of lower overall survival [22]. hnRNPM (heterogeneous nuclear ribonucleoprotein M) inhibits GC metastasis by regulating gene AS during cell migration [23]. However, the mechanism by which FRGs undergo dysregulation of splicing components in GC remains unknown. Studying the characteristics and biological activities of FRAs is crucial for improving the treatment and prognosis of GC.

Although considerable study has been conducted on the full transcriptome of AS events, there are no studies that demonstrate how FRAs impact GC. In this study, the percent spliced-in (PSI) value was utilized to determine the prognostic value of FRAs, leading to the creation and validation of an FRA prognostic signature. We examined the characteristics of FRAs in relation to TME cell infiltration, targeted therapy, and immunotherapy. Using correlation analysis and in vitro experiments, we verified the regulatory axis between SF3A2 and FBXW7|70846|AP in SFs and FRAs, respectively. Overall, these results revealed that FRAs could be exploited as novel prognostic indicators, opening new research avenues into the molecular mechanisms underlying FRA occurrence in GC and their therapeutic applications.

2. Materials and methods

2.1. Data preprocessing and collection

GC patient transcriptome and clinical data were retrieved from the TCGA online database (https://portal.gdc.cancer.gov/), obtaining a total of 447 GC tissue samples. After excluding patients with inadequate clinical information, insufficient statistics, and short-term follow-up events, 406 GC samples remained for data analysis. The FRG collection was sourced from the FerrDb database (http://www.zhounan.org/ferdb/), the first online portal dedicated to ferroptosis and disease connections. Ferroptosis-promoting and ferroptosis-inhibiting factors were obtained and combined into a single set. After removing duplicate genes from driver and suppressor sets, the FRG gene set included 217 genes. To ensure the reliability of the AS events, we quantified them using PSI values and filtered out those with PSI values below 0.75. The default format for specifying AS events was gene symbol - AS ID - AS type. AS events included alternative acceptor sites (AA), alternative donor sites (AD), alternative promoters (AP), alternative terminators (AT), exon skipping (ES), mutually exclusive exons (ME) and retained intron (RI). With AS events controlled, we collected the gene symbols of 404 SFs for data analysis [24]. R version 4.1.0 was used to collect and analyze all raw data.

2.2. Identification of FRGs and FRAs in GC

The "AnnoProbe" package was utilized to relabel the R-based gene sequence matrix, the 'limma' package was employed to calibrate the microarray data, and the "UpSetR" package was utilized to convert the gene distribution over the seven AS events into a graphical representation [25]. Using univariate Cox regression analysis, the impact of each AS event PSI on the clinical outcome of GC patients was determined, ultimately revealing OS-associated AS occurrences. Then, for OS-associated DEAS events, we used the "UpsetR" package to characterize the relevant AS events of the parental genes. A P-value <0.05 indicated statistical significance.

2.3. AS events with anticipated FRG construction

For OS-AS events screened by univariate Cox regression analysis, LASSO regression analysis was used to create a generalized linear signature while adjusting for variables and complexity [26]. The AS occurrences evaluated by LASSO regression were then subjected to multifactor Cox regression analysis to develop a risk signature. Using the signature, risk scores were produced for each GC patient based on the median risk scores: Risk score = $\sum$Expi * βi (Expi, each FRG's signature expression; βi, each PRG's signature coefficient).

Patients were separated into high- and low-risk groups. The signature's capacity to predict the outcome of GC patients was determined using Kaplan-Meier survival analysis curves and receiver operating characteristic (ROC) curves [27]. Additionally, we conducted univariate and multivariate Cox regression analyses on the risk score, gender, age, TNM stage, and tumor grade.

2.4. Analysis of the clinical importance and stratification ability of the prognostic signature

Stratification analyses were used to reduce confounding variables and identify the specific link between risk scores and GC patients. According to clinicopathologic features, including age, gender, stage M, stage N, tumor stage, tumor grade, and stage T, we separated GC samples into distinct layers. This allowed us to investigate the relationship between exposure to the AS signature and each layer, determining the main performance of the AS signature in GC patients.

2.5. Construction and validation of a clinical prediction nomogram

We employed univariate Cox and multivariate regression analyses to identify independent prognostic markers. A nomogram prediction signature for 1-year, 3-year, and 5-year overall survival (OS) was established using the "rms" R package. The accuracy of the predicted survival probabilities was validated using 1-, 3-, and 5-year calibration plots, while the performance of the nomogram was evaluated using time-dependent ROC [28].

2.6. Functional enrichment analysis

First, we selected 436 FRAs connected to differentially expressed genes (DEGs) with absolute values of $|\text{Log2 FC}| > 0.58$ and $p < 0.05$ associated with the two risk categories. The "ClusterProfiler" package [29] was then used to perform Gene Ontology (GO) analysis, including the biological process (BP), cellular component (CC), and molecular function (MF) categories. Additionally, Kyoto Encyclopedia of Genes and Genomes (KEGG) analyses were conducted using the same package.

2.7. Evaluation of TME infiltration, immunological checkpoints, and medication sensitivity between low- and high-risk groups

The immunological and stromal scores of the TME were analyzed using the ESTIMATE method. The infiltration of 22 human immune cell types was computed for each patient using the CIBERSORT program [30]. The single-sample gene set enrichment analysis (ssGSEA) technique was used to evaluate the scores of invading immune cells and the activity of immune-related pathways, utilizing the "GSVA" R package [31]. Additionally, the connections between the two subtypes and the expression of 47 immunological checkpoints was evaluated [32,33]. The "pRRophetic" R program was utilized to predict the half-maximal inhibitory concentration (IC50) values of chemotherapeutic medicines [34]; the immunophenoscore (IPS) values for CTLA-4 and PD-1 inhibitors were obtained from the TCIA database. Two score groups were predicted for PD-1 and CTLA4 were predicted using the TIDE algorithms (http://tide.dfci.harvard.edu/) [35].

2.8. SF and FRA network development

The mRNA expression data of 404 SFs were obtained from TCGA. All SF expression levels and PSI values of the 12 FRAs were ranked for each variable. After calculating the square of each difference in rank between the two groups, Spearman rank correlation analysis (Cor >0.4, FDR <0.05) was conducted. Fifteen SFs were detected with a high correlation to 2 FRAs. Based on the risk value of each FRA, a network of SF-FRA-risk/protection was constructed.

2.9. Quantitative RT–PCR analysis to measure FRA expression

We selected the SF-AS pair with the highest correlation from the regulatory network. To ensure the validity of the experimental results, the following forward and reverse primers were designed: SF3A2 (Forward 5′-TCG ACA TCA ACA AGG ACC CG-3′, Reverse 5′-GCT TCT TCC CCT GCG TAT GT-3′), FBXW7|70846|AP (Forward 5′-CAG GAC ATT TGG TAG GGG AAG G-3′, Reverse 5′-GGA GGC CTT GGG CAA TGA T-3′), and GAPDH (Forward 5′-TCG GAG TCA ACG GAT TTG GTC-3′, Reverse 5′-ATG GAA TTT GCC ATG GGT GGA-3′). On an Applied Biosystems 7900HT Sequence Detection System, mRNA expression was evaluated using SYBR Green qPCR MasterMix (Seven, China). Relative mRNA changes were calculated using the $2^{-\Delta\Delta Ct}$ method, with GAPDH serving as the internal standard. Each measurement was performed in triplicate. We also utilized agarose gel electrophoresis to evaluate the expression of the transcripts measured by PCR.

2.10. Culture, treatment, and transfection of cells

The human gastric cancer AGS (CL-0022) and HGC-27 (CL-0107) cell lines were supplied by Procell Biocentre (Wuhan, China). Cells were cultured in F–12K/DMEM (Procell, China) supplemented with 10 % fetal bovine serum (Biological Industries, Israel). Using siRNA (Guangzhou, China), the cellular expression of SF3A2 (GCCTGACACTTCACAACAA) was temporarily suppressed. NC siRNA (Guangzhou, China), which has no effect on gene knockdown, was employed as a control. The pcDNA3.1 plasmid vector (Changsha, China) was used to overexpress SF3A2 mRNA. Before the day of transfection, 2×10^5 cells were seeded into each well of a 6-well plate

to achieve 50 % confluency. 50 nM siRNA was diluted into 200 μl jetPRIME® buffer, then 4 μl jetPRIME® reagent was added, vortex for 1 s, after 15 min of incubating, the mixture was evenly distributed across the well. All cells were cultured in an incubator (Thermo Scientific, US) at 37 °C in a humidified 5 % CO_2 environment. As previously described, a ferroptosis inducer containing 10 μM erastin [36,37] was applied to cells grown in six-well plates.

2.11. Cell proliferation assay

Cell Counting Kit-8 (CCK-8) Assay. Different groups were established with 4×10^3 cells per well in 96-well plates. Four 96-well plates were used with five replicate wells for each group. At 0 h, 24 h, 48 h, and 72 h, 10 μl of CCK-8 reagent was added to the wells. After 2.5 h in an incubator at a constant temperature of 37 °C, the optical density (OD) was measured at 450 nm.

EdU Assay. Separate groups of treated cells were seeded into 12-well plates at a density of 5×10^4 cells per well, and the cells were incubated for 2 h at 37 °C in complete medium containing EdU (10 μM) (Beyotime, China). Then, the cells were fixed for 15 min in 4 % paraformaldehyde. For permeabilization, 500 μl of 0.3 % Triton X-100 PBS (Beyotime, China) was added to each well for 15 min. The cells were stained with Click-reaction solution (Beyotime, China) for 30 min, followed by DAPI (Beyotime, China) staining for 5 min. Each well was meticulously washed and imaged under an inverted fluorescence microscope.

2.12. ROS detection

DCFH-DA (Beyotime, China) was diluted 1:1000 in serum-free growth medium (Procell, China) to a final concentration of 10 μmol/L. This solution was then added to 6-well plates containing cells grown to 90 % confluency. After 30 min of incubation, the fluorescence intensity was assessed under a fluorescence microscope.

2.13. Colorimetric intracellular iron assay

To wash cells in a 24-well plate, prechilled PBS was used. Then, 200 μl of lysis solution was added to each well, and the plate was shaken for 2 h. Mix A (Applygen, China) was prepared by mixing the kit's dilution solution and a 4.5 % potassium permanganate solution in a 1:1 ratio. At 60 °C, 100 μl of Mix A was incubated with 100 μl of sample for 1 h. Then, 30 μl of iron ion detector was added, and the plate was incubated at room temperature for 30 min. Finally, the absorbance at 550 nm was measured using 200 μl from 96-well plates. The reaction product was measured according to the manufacturer's protocol.

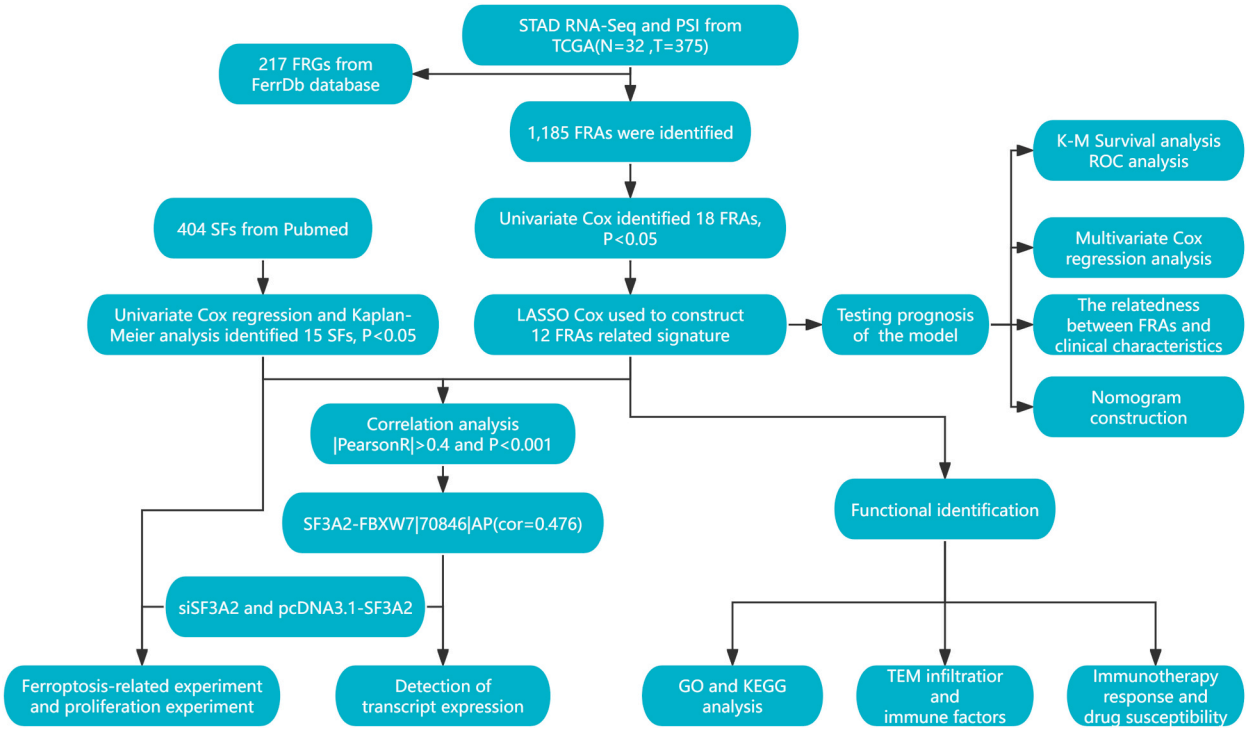

Fig. 1. | Flow diagram of FRA as prognostic marker.

2.14. Immunofluorescence assay

The day before the experiment, cells were seeded in 6-well plates with glass slides. The next day, 1 ml of 4 % paraformaldehyde was applied to each well for 20 min at room temperature. After three washes with PBS, 1 ml of 0.5 % Triton X-100 (Beyotime, China) was applied to each well to permeabilize the membrane. For cell blocking, 2 % bovine serum albumin (BSA) (Shanghai, China) was used. Anti-Ki67 (1:150 dilution, Wuhan, China) was employed for staining. The diluted antibodies and cells were mixed overnight at 4 °C and then incubated for 1 h at room temperature with secondary antibodies (Beijing, China). Finally, photographs were taken using a fluorescence microscope.

2.15. Statistical evaluation

R (version 4.1.0), GraphPad Prism (version 9.0), and SPSS software were utilized for all statistical analyses (23.0). $P < 0.05$ was regarded as statistically significant for all analyses.

3. Results

3.1. Overview of FRAs and screening for AS events related to survival in gastric carcinoma

The full flow of the research is described in Fig. 1. Identifying the splicing taxonomic features of FRGs and understanding the AS landscape of all genes are crucial for comprehending the transcriptional regulation of FRGs. AS events were scattered among seven common splice types: including alternate acceptor site (AA), alternate donor site (AD), alternate promoter (AP), alternate terminator (AT), mutually exclusive exons (ME), retained intron (RI), and exon skip (ES) (Fig. 2A). We obtained 217 FRGs from the FerrDb database and identified 1185 AS events. A total of 555 ES events were performed on 155 genes, making ES the most frequent splicing event. The other splicing events, in descending order of occurrence, were AP, AT, AA, AD, RI, and ME. This suggests that AS does not occur randomly; instead, there is a preference for certain splicing types (Fig. 2B). A total of 159 FRGs underwent multiple AS events,

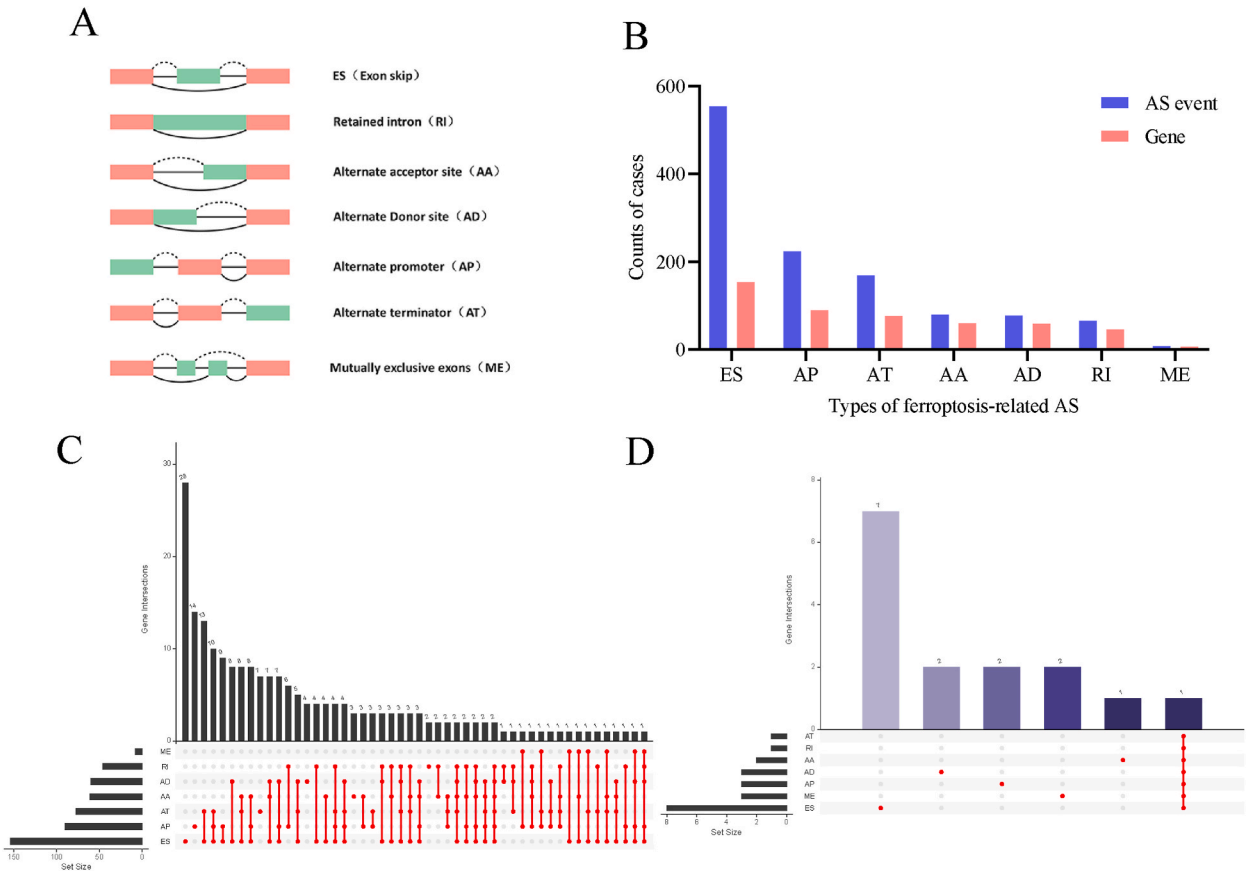

Fig. 2. | An overview of FRAs events in GC. (A) 7 different types of AS events. (B) The number of FRAs and parental genes counted according to AS event types. (C) UpSet plot, it shows the signature of AS events in parental genes. (D) UpSet plot of interactions between prognostic FRAs and its parent genes.

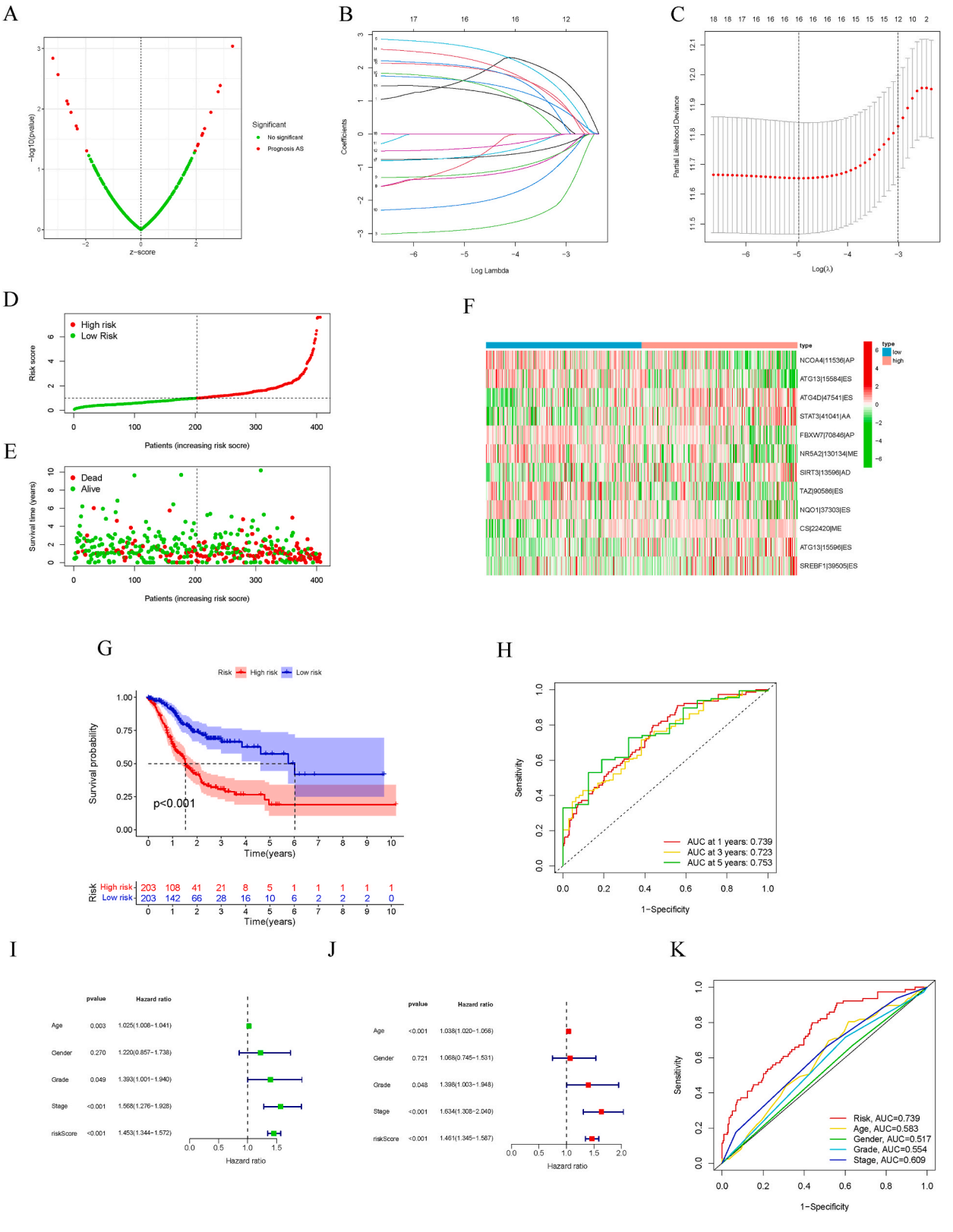

(caption on next page)

Fig. 3. | Prognostic AS signature was constructed and independent prognostic factors were identified in GC. (A) Volcano map for prognostic FRAs events. (B, C) In the LASSO-Cox model of TCGA-STAD cohort, the minimum standard was adopted to obtain the value of the super parameter λ by 10-fold cross-validation. The λ value was confirmed as 0.07685 where the optimal lambda resulted in 12 non-zero coefficients. (D) Risk score map, grouping GC patients according to the median of risk score. (E) The survival of GC patients in different groups. (F) Heat map showing the expression of 12 AS events in two groups. (G) Kaplan-Meier curves with log-rank test for GC patients. (Log-rank test, $p < 0.001$). (H) The AUC of time-dependent ROC curves based on risk score. (I, J) The univariate and multifactorial Cox regression analysis for clinicopathologic features. (K) ROC curves of independent prognostic factors.

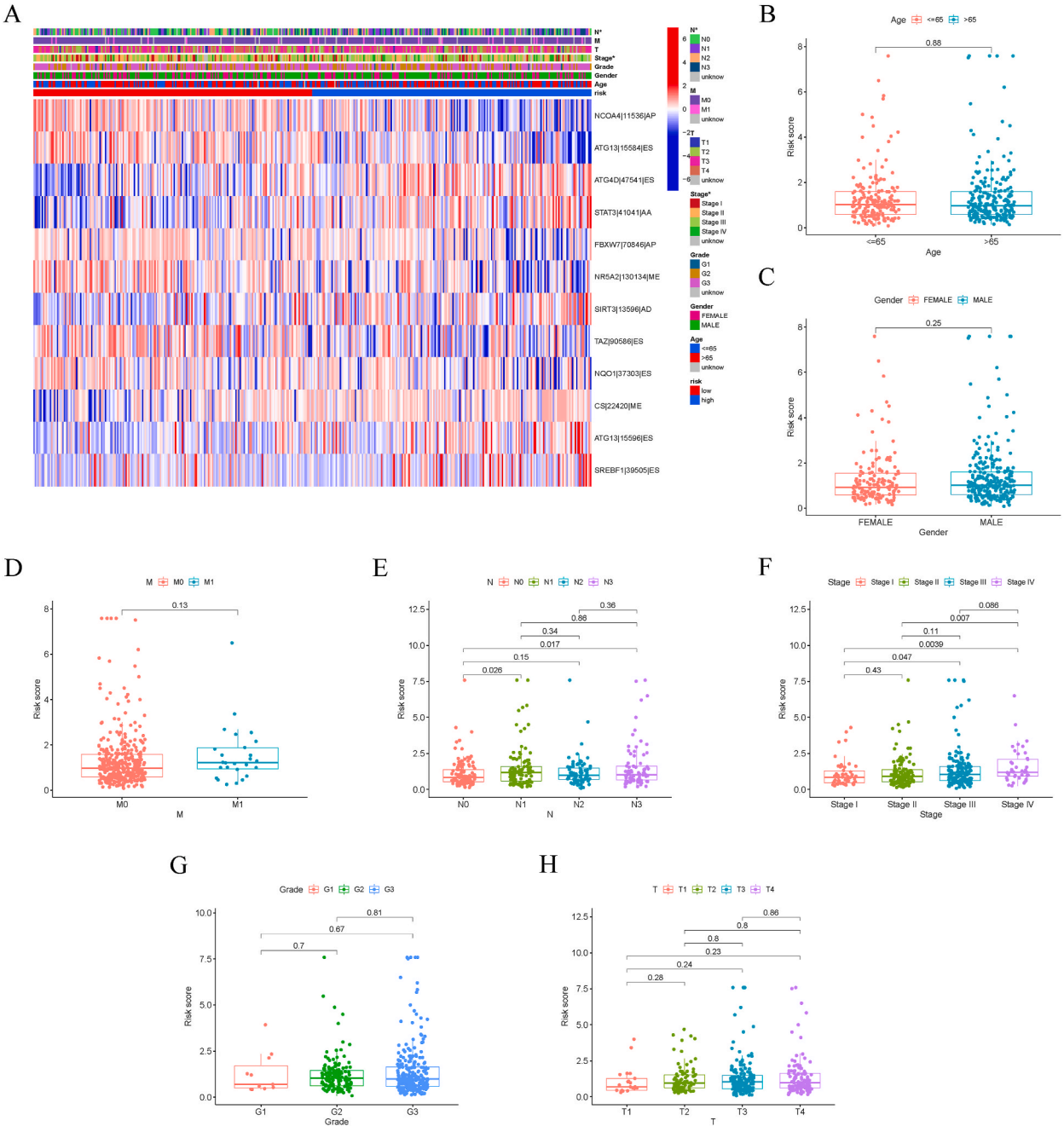

Fig. 4. | The association between FRAs signature and the clinicopathological features in GC. (A) Heat map of clinicopathological features in high- and low-risk groups in GC (Chi-square test or Fisher's exact test, $*P < 0.05$; $**P < 0.01$; $***P < 0.001$). (B–H) Box diagram representation for different risk groups in terms of clinicopathological characteristics, (Wilcox test, $*P < 0.05$; $**P < 0.01$; $***P < 0.001$).

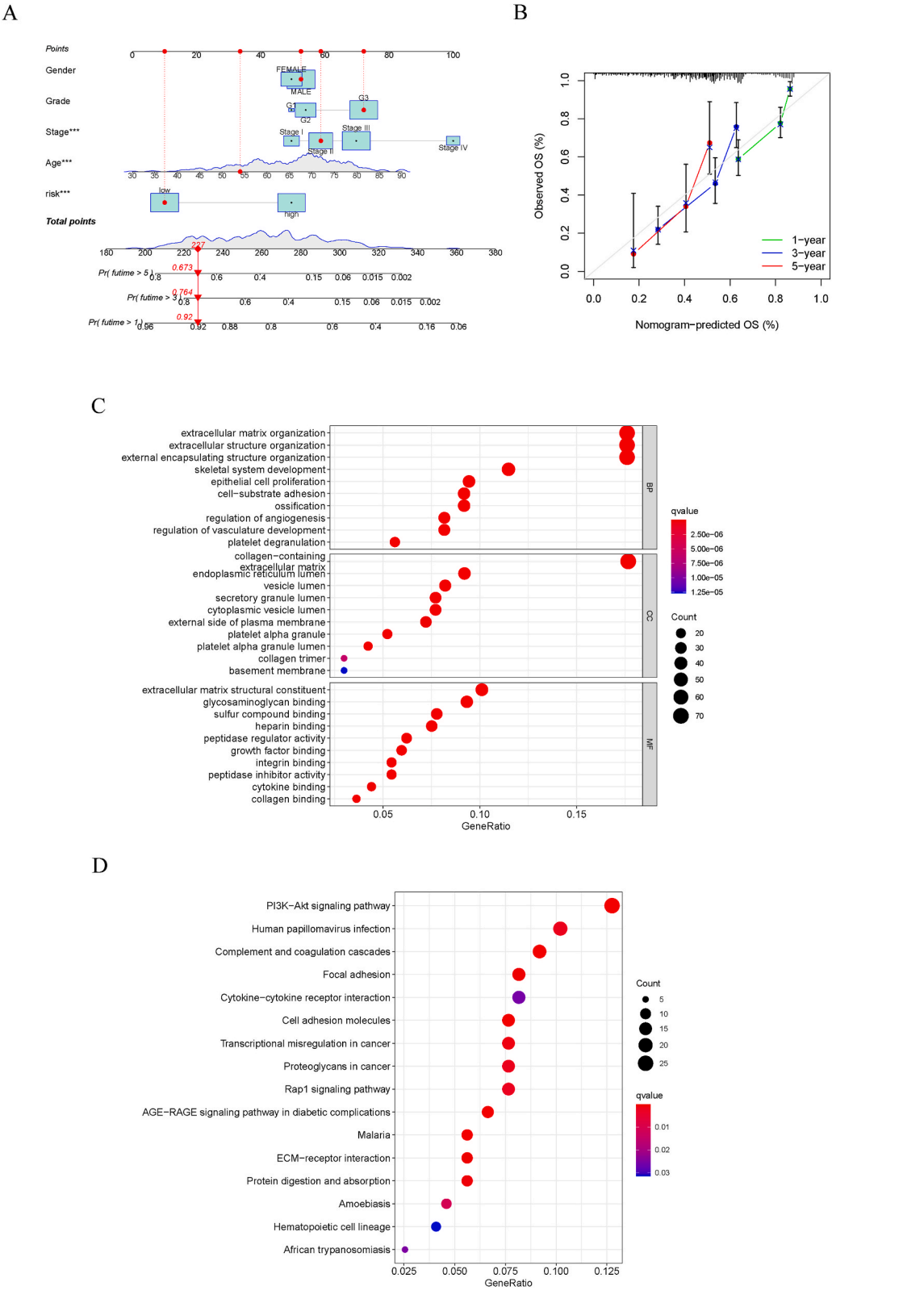

(caption on next page)

Fig. 5. | Nomogram predict survival for GC patients and the biological function and pathway in AS signature. (A) Nomogram constructed by risk scores and clinicopathological features is employed to predict the prognosis of GC patients. (B) The calibration plot of AS signature and clinicopathological features. (C) GO enrichment analysis of biological processes enriched in different groups. (D) KEGG pathway enrichment analysis of the differentially expressed genes grouped by AS signature. (Bayes moderation, $*P < 0.05$; $**P < 0.01$; $***P < 0.001$).

produced far more than two transcripts. The different AS types of FRAs were visualized in UpSet plots (Fig. 2C). Univariate Cox regression analysis was used to identify prognostic AS events among the 1185 FRAs. We found that 18 AS events were significantly associated with OS in GC patients ($p < 0.05$). We discovered that only one parental gene for prognostic AS events had more than two splice types. Prognosis-related transcripts were often one of several transcripts of parental genes (Fig. 2D).

3.2. Development and evaluation of AS-based prognostic signature

We marked prognostic AS events with red dots in the volcano plot (Fig. 3A). LASSO regression and multivariate analysis were employed to identify for independent prognostic factors in GC based on 18 AS events, leading to the identification of 12 FRAs (Fig. 3B–C) including NCOA4|11536|AP, ATG13|15584|ES, ATG4D|47541|ES, STAT3|41041|AA, FBXW7|70846|AP, NR5A2|130134|ME, SIRT3|13596|AD, TAZ|90586|ES, NQO1|37303|ES, CS|22420|ME, ATG13|15596|ES, and SREBF1|39505|ES were identified. The characteristics of their AS type in (Fig. S. 1). An AS signature was built from these 12 FRAs, and a formula based on the signature's characteristics and regression coefficients was established to calculate patient risk scores using the following formula: risk score = NCOA4|11536|AP * (−2.84672098471663) + ATG13|15584|ES * (−3.7739758802168) + ATG4D|47541|ES * 1.73957177191192 + STAT3|41041|AA * 2.67659067668673 + FBXW7|70846|AP * (−1.30368835410691) + NR5A2|130134|ME * (−0.926863953619284) + SIRT3|13596|AD * 2.26136568357004 + TAZ|90586|ES * (−1.23847007753781) + NQO1|37303|ES * (−2.54089884699231) + CS|22420|ME * 2.80619789869434 + ATG13|15596|ES * 1.74428023840916 + SREBF1|39505|ES * 2.48852689381684. Following the calculation of each patient's risk score, the median risk score was used to divide patients into a high-risk group (n = 203) and a low-risk group (n = 203) for further analysis. The risk curve ranked the patients' risk scores (Fig. 3D). The high-risk group had significantly worse overall survival than the low-risk group (Fig. 3E). Among the FRAs included in the signature, NCOA4|11536|AP, ATG13|15584|ES, FBXW7|70846|AP, NR5A2|130134|ME, TAZ|90586|ES, and NQO1|37303|ES had significantly lower expression levels in the high-risk group (Fig. 3F). K-M survival curves revealed that patients in the high -risk group were more likely to have poor clinical outcomes than those in the low-risk group (Fig. 3G). Furthermore, ROC curves revealed the AS module's forecasting capability for the prognosis of GC patients, with 1-year, 3-year, and 5-year area under the curve (AUC) values of 0.739, 0.723, and 0.753, respectively (Fig. 3H). These analyses validated the AS signature's exceptional prognostic ability for GC patients. Additionally, we discovered that risk score (HR: 1.461, 95 % CI: 1.345–1.587), grade staging (HR: 1.398, 95 % CI: 1.003–1.948) and tumor stage (HR: 1.634, 95 % CI: 1.308–2.204) were independent prognostic factors for GC (Fig. 3I–J). The AUC of the risk score for predicting 3-year survival in GC patients was 0.739, which was higher than those of the Garde score (0.554), age (0.583), gender (0.517), and stage (0.609) (Fig. 3K). These findings showed that the risk signature, alone or in combination with other graded indicators, outperformed other factors in predicting the prognosis of GC patients.

3.3. The AS prognostic Signature's expression and clinical features

We correlated risk scores with GC clinicopathological characteristics, and the results showed that the risk scores were consistent across different stratifications. Six FRAs were identified as risk factors, and their expression levels were higher in the high-risk group. Others demonstrated protective function in GC and were downregulated in the high-risk group. When comparing the clinicopathological characteristics of the two groups, significant differences were found in tumor stage and N stage (Fig. 4A). Furthermore, stages III-IV were significantly enriched in the high-risk group, and the risk scores of GC patients with N stages 1–3 were higher. However, some clinicopathological characteristics, such as age, gender, M stage, tumor grade, and T stage, showed differences between the high- and low-risk groups, but these differences were not significant (Fig. 4B–H). We also determined the OS of GC patients grouped by AS signature and further subgrouped by different clinicopathological features. Notably, the low-risk group had better OS than the high-risk group in the subgroups of age, gender, tumor grade, M stage, N stage, tumor stage, and T stage (Fig. S. 2A-2G). However, there was no significant difference in OS in the M1 subgroup (Fig. S. 2D). According to the findings of these studies, the AS signature may have a meaningful impact on predicting tumor progression.

3.4. Defining the composite prognostic nomogram and functional enrichment of the high- and low-risk groups

The predictive nomogram calculates a patient's chance of survival by adding the scores of many relevant factors identified on a point scale. Four variables, including age, lymph node metastasis, TNM staging, and OS signature, were eventually included in the subsequent OS nomogram construction using backward stepwise selection based on optimized Akaike's information criterion (AIC) (Fig. 5A). The calibration plot supports the nomogram's accuracy (Fig. 5B). As a result, the nomogram combining clinical characteristics and risk scores had a more accurate predictive function and could be used to assess GC patients' clinical prognosis. The performance of the risk signature, as well as the molecular mechanisms and functional roles of FRAs, were investigated in the two groups. Functional enrichment analyses were conducted on the mRNA expression levels of sample genes in the two risk groups. GO and KEGG enrichment analyses were performed, revealing that the extracellular matrix was present in all CC, MF, and BP categories in the

high-risk group by GO analysis. Differential genes were significantly enriched in processes related to cell substrate adhesion, epithelial cell proliferation, angiogenesis regulation, growth factor binding, and cytokine binding (Fig. 5C). Furthermore, the KEGG analysis revealed that the most frequently enriched pathways were the PI3K-Akt signaling pathway, transcriptional misregulation in cancer,

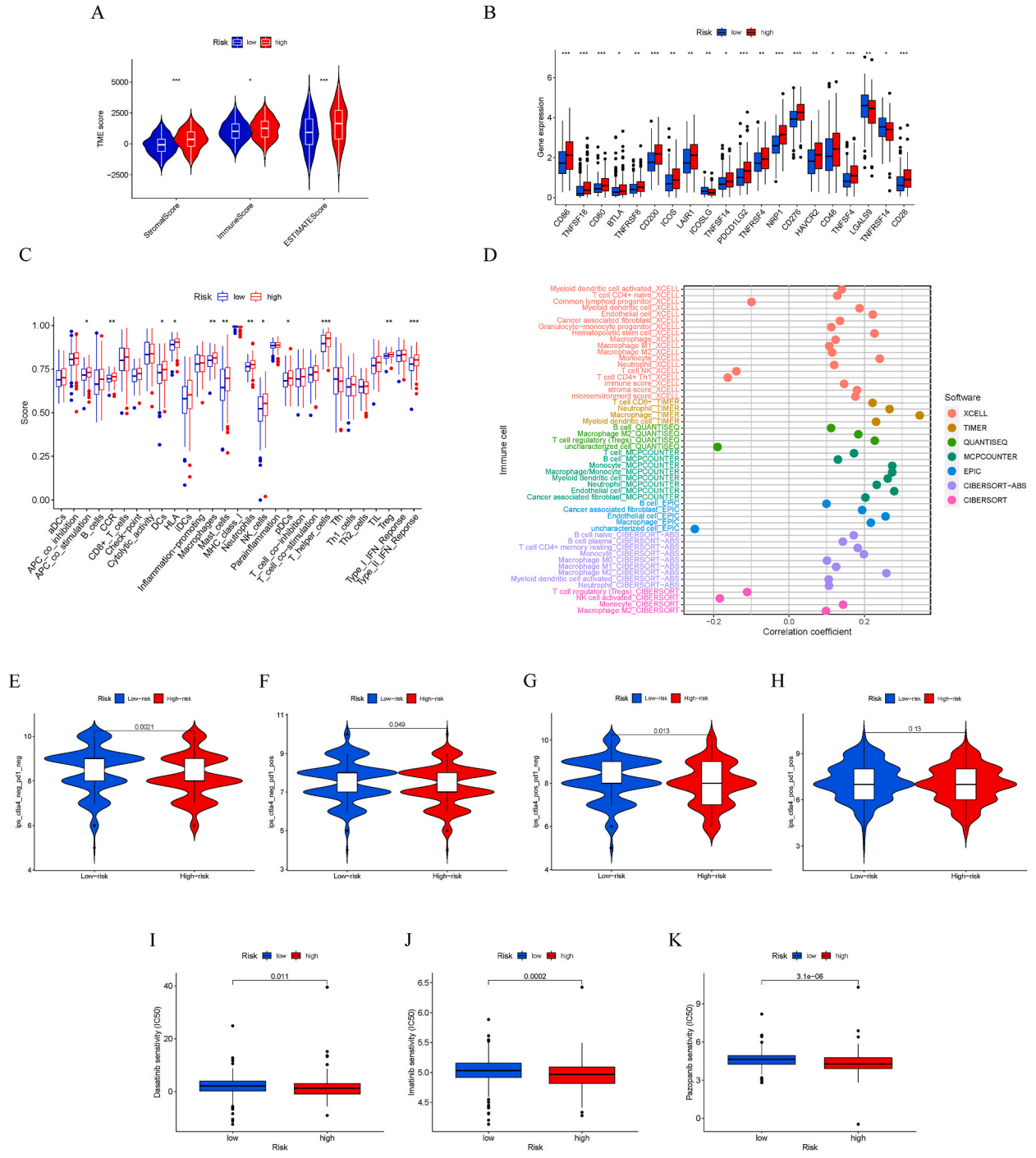

Fig. 6. | Immune infiltration in the high- and low-risk groups in GC. (A) The two groups of Immune score, stromal score, tumor purity in GC patients (Wilcox test, $*P < 0.05$; $**P < 0.01$; $***P < 0.001$). (B) Box diagram indicates the different immune abundances in the high- and low-risk groups. (Wilcox test, $*P < 0.05$; $**P < 0.01$; $***P < 0.001$). (C) Expression of immune-related genes in GC among two groups based on AS signature. (Wilcox test, $*P < 0.05$; $**P < 0.01$; $***P < 0.001$). (D) XCELL, TIMER, QUANTISEQ, MCPCOUNTER, EPIC, CIBERSORT−ABS, CIBERSORT algorithms is used to calculate the correlation between immune cells and GC patient samples. (E–H) The response of the groups to immunotherapy according to anti-CTLA-4 and anti-PD-1. (Wilcox test, $*P < 0.05$). (I–K) Sensitivity of the two groups to different targeted drugs. (Wilcox test, $*P < 0.05$).

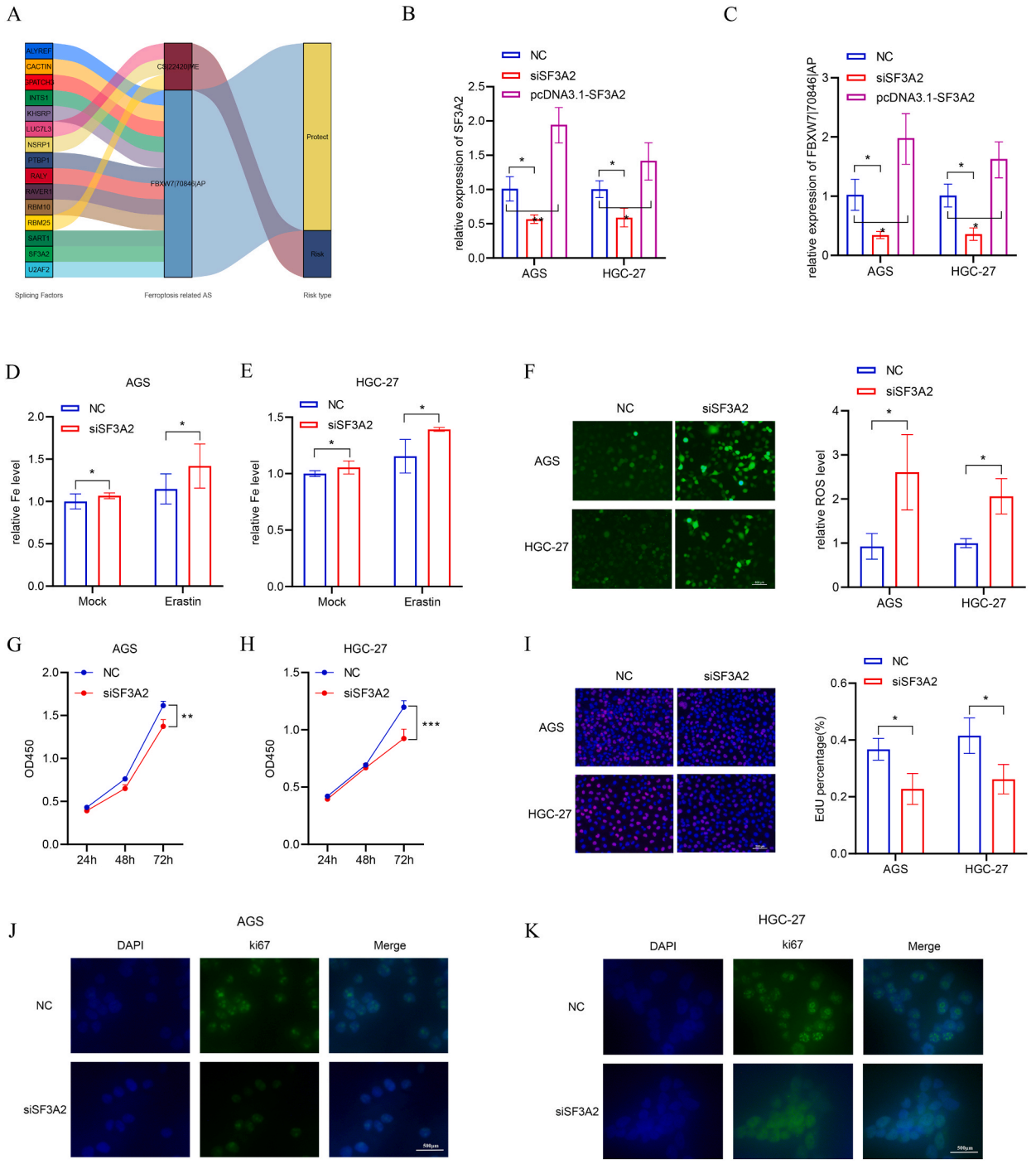

Fig. 7. | SF3A2 regulates the AS of FBXW7 pre-mRNA. And SF3A2 reduces cytoplasmic peroxidation and inhibits ferroptosis, while promoting the proliferation of GC cells. (A) The Sankey diagram identified the coherence and potential relationship between SFs and FRAs. (B) qPCR reveals the knockdown and overexpress efficiency of SF3A2 in cells (Paired *t*-test, $^{*}P < 0.05$; $^{**}P < 0.01$). (C) qPCR indicated the expression of FBXW7|70846|AP in gastric cells. (D, E) Detection of total iron ion alterations in siSF3A2 GC cells (Paired *t*-test, $^{*}P < 0.05$; $^{**}P < 0.01$; $^{***}P < 0.001$). (F) Differential performance for ROS in the NC and siSF3A2 groups, right bar chart represents quantification relative level of ROS (Paired *t*-test, $^{*}P < 0.05$; $^{**}P < 0.01$; $^{***}P < 0.001$). (G, H) CCK-8 assay indicates cell proliferation at 24,48,72 h (Paired *t*-test, $^{*}P < 0.05$; $^{**}P < 0.01$; $^{***}P < 0.001$). (I) The EdU assay shows the amount of new GC cells added at 2 h, with quantitative results of the bar chart right (Paired *t*-test, $^{*}P < 0.05$; $^{**}P < 0.01$; $^{***}P < 0.001$). (J, K) Immunofluorescence exhibits the location and abundance of ki67 in NC and siSF3A2 cells. (Paired *t*-test, $^{*}P < 0.05$; $^{**}P < 0.01$; $^{***}P < 0.001$).

proteoglycans in cancer, cell adhesion molecules, ECM receptor interaction, protein digestion and absorption, Rap1 signaling pathway, and cytokine–cytokine receptor interaction (Fig. 5D).

3.5. Immune cell infiltration examination

We sought to evaluate the relationship between AS signature characteristics and antitumor immunity by comparing the abundance of infiltrating immune cells between the two groups. Stromal scores, immune scores, and estimation scores were all markedly higher in the high-risk group (Fig. 6A). Immune checkpoint gene expression levels in high-risk and low-risk GC patients were determined, revealing that 20 checkpoint genes differed significantly between the two groups. In the high-risk group, 19 immune-related genes were highly expressed (Fig. 6B). Furthermore, we calculated scores for the functional activity of 19 immune cells and 10 immune-related functions in the two groups. In the high-risk group, the abundances of Treg cells, DCs, HLA, macrophages, mast cells, neutrophils, NK cells, pDCs, T helper cells, APC costimulation, type II IFN response, and other immune cells and immune-related pathways were higher (Fig. 6C). We analyzed the correlation coefficients of immune cells with GC patients using seven different algorithms, including XCELL, TIMER, QUANTISEQ, MCPCOUNTER, EPIC, CIBERSORT-ABS, and CIBERSORT. In the high-risk group, there were higher abundances of macrophages, monocytes, myeloid dendritic cells, naive $CD4^+$ T cells, and $CD8^+$ T cells, while the correlations with $CD4^+$ Th1 T-cell, activated NK cell, and uncharacterized cell correlations were also lower (Fig. 6D). The patients were then divided into four subgroups based on their response to anti-CTLA-4 and anti-PD-1 immunotherapy. The low-risk group responded better to immunotherapy in the CTLA-4-positive PD-1-negative, CTLA-4-negative PD-1-negative, and CTLA-4-negative PD-1-positive subgroups. However, there was no significant difference between the two groups in the CTLA-4-positive PD-1-positive subgroup (Fig. 6E–H). We also compared the sensitivity to common molecularly targeted drugs between the two groups, with dasatinib, imatinib, and pazopanib showing a significant increase in sensitivity in the low-risk group (Fig. 6I–K).

3.6. Transcriptional differences in FBXW7 are closely related to SF3A2

The biological process studied, namely direct binding of SFs to pre-mRNA, was influenced by exon selection and splice site strength to regulate the AS type of genes. Therefore, we investigated the expression of 404 SFs in GC patients and connected them with the 12 FRAs used for the prognostic signature. Ultimately, 15 SFs were discovered to be associated with 2 AS events, FBXW7|70846|AP and CS|22420|ME (Fig. 7A). The AS event FBXW7|70846|AP was a protective factor, whereas the AS event CS|22420|ME was a risk factor. ALYREF, CACTIN, GPATCH3, INTS1, KHSRP, PTBP1, RALY, RAVER1, RBM10, SART1, SF3A2, and U2AF2 might regulate FBXW7|70846|AP. CS|22420|ME might be regulated by 3 SFs including LUC7L3, NSRP1, and RBM25. SF3A2 was found to be positively related to FBXW7|70846|AP. Interestingly, SF3A2 was also associated with FBXW7|70849|AP (Table S. 1), suggesting that SF3A2 might have a closer biological relationship with FBXW7. We selected the highest correlation for verification by biological analysis. siRNA and Plasmid DNA were used to regulate the expression of SF3A2 in AGS cells and HGC-27 cells, and the gene knockout efficiency was confirmed by qPCR (Fig. 7B). qPCR revealed that the FBXW7|70846|AP level was reduced in the siSF3A2 group compared with the normal control group. However, the expression level of FBXW7|70846|AP was increased in the overexpression group. These results indicated a positive regulatory effect of SF3A2 on FBXW7|70846|AP, which was consistent with our bioinformatic analysis results (Fig. 7C, Fig. S. 3).

3.7. Knockdown of SF3A2 reduces cellular resistance to ferroptosis and inhibits GC cell proliferation

We attempted to knockdown SF3A2 and observe whether cells underwent iron-dependent death to analyze the specific effect of AS on ferroptosis. Before conducting this study, we compared the differences in SFs between the low- and high-risk groups of GC patients. The findings revealed that these SFs were abundant in tumors (Fig. S. 4A). Box plots showed the same results, with SF3A2 being more abundant in high-risk samples than in low-risk samples (Fig. S. 4B). We identified the importance of SF3A2 in ferroptosis regulation. The total iron ion content of cells was measured in siSF3A2 cells and NC cells treated with 10 μM erastin, and siSF3A2 cells produced more total iron ions (Fig. 7D and E). ROS levels were also measured, with siSF3A2 cells having higher levels (Fig. 7F). Ferroptosis inhibits cell proliferation and can be induced by compounds such as erastin, a Ras-selective lethal small-molecule drug [38]. Therefore, we measured the cell proliferation capacity using the CCK-8 reagent, and the tumor cell proliferation capacity of siSF3A2 cells was significantly reduced (Fig. 7G and H). The same results were obtained with EdU testing (Fig. 7I). To further clarify the effect of SF3A2 on GC cell proliferation, we performed immunofluorescence staining for Ki67 in the cells. The cellular Ki67 expression levels in AGS and HGC-27 cells were decreased after SF3A2 knockdown (Fig. 7J and K). According to the findings, SF3A2 inhibited cell proliferation and decreased ferroptosis resistance in cells.

4. Discussion

In GC, the probable mechanisms of FRGs are not well characterized or clarified. AS generates numerous proteins from a single gene, thereby enhancing proteome diversity [18]. AS leads to the production of significantly more transcripts than genes, and these FRAs play a crucial role in the ferroptotic process. However, few studies have examined the role of AS in ferroptosis.

In this study, we focused on the role of AS in the potential for ferroptosis induction and investigated the biological activities of FRAs in GC. Identifying variable FRAs could enhance the understanding of the ferroptosis process and provide an approach for individualized therapy. A total of 18 prognostic AS events were identified from 1185 FRAs in 406 GC samples, and 12 FRAs were used to

develop an effective risk AS signature for predicting the OS of GC patients according to the PSI value. Univariate Cox regression, multivariate Cox regression, and systems biology techniques determined that the AS signature had independent prognostic value for GC patients and exhibited stronger predictive performance than the TNM stage. We discovered that two of the 12 FRAs, ATG13|15584|ES and ATG13|15596|ES, are derived from the same parent gene. Notably, ATG13|15584|ES was part of the protective AS signature, whereas ATG13|15596|ES was a risk FRA. Furthermore, we created an SF-AS coexpression network and found that SF3A2 had strong associations with FBXW7|70846|AP, a protective prognostic FRA. We investigated the functional enrichment of differentially expressed genes in high-risk and low-risk GC patients to determine the functional and molecular mechanisms of FRAs. Both groups were heavily involved in the initiation and maintenance of GC. For example, angiogenesis may influence the creation and balance of the TME, potentially leading to hypoxia [39]. ROS and angiogenesis are also connected, suggesting a potential relationship between angiogenesis and ferroptosis [40]. The PI3K-AKT signaling pathway was highly enriched in the high-risk group. PI3K and AKT mid-regulators promote cellular proliferation and tumorigenesis via oncogenic signaling and metabolic reprogramming [41]. When the PI3K/AKT pathway is activated, it blocks ferritin autophagy and hence iron-dependent lipid peroxidation [42]. The study "Transcriptional dysregulation in cancer" found that AS expression differed across high- and low-risk groups, indicating that AS might be associated with tumor grade malignancy [43]. Cell adhesion molecules and the Rap1 signaling pathway, both linked to cancer metastasis, were also shown to be enriched [44,45]. Proteoglycans influence cancer cell behavior and the TME during the evolution of solid tumors and hematopoietic malignancies [46], implying that ferroptosis may function in an alternate tumor pathway [47]. These findings underscore the predictive capacity of the FRA-based signature and indicate a possible mechanism for the partial stimulation or suppression of ferroptosis in GC.

Ferroptosis is a TME regulator, and ferroptosis inducers can promote lipid peroxidation in immune cells, limiting their function and survival [48]. In vivo, $CD8^+$ T lymphocytes can cause ferroptosis in tumor cells [49]. By reducing ferroptosis in Treg cells, GPX4 maintains TME homeostasis [50]. Treg and CCR cells were found to be strongly related to FRGs in one investigation [51]. This result suggested that immunotherapy could benefit low-risk GC patients. Ferroptosis in tumor or immune cells promotes the establishment of an immunological milieu via numerous pathways, and ferroptosis plays a crucial role in immunity. Macrophages regulate ferroptosis in tumor cells biologically; therefore, modifying macrophage activity could be a cancer treatment strategy [52]. We discovered that macrophages were considerably overrepresented in high-risk patients. Furthermore, by inducing macrophage polarization, tumor cell ferroptosis increases proliferation and spread [53]. As a result, targeting macrophages may have an impact on the tumor immune microenvironment. Some oncogenic pathways can induce ferroptosis in carcinoma cells, raising their potential in cancer therapy [54]. The high-risk group was found to be less sensitive to dasatinib, imatinib, and pazopanib. Sun and colleagues observed that suppressing cellular ferroptosis increased sorafenib resistance, which is consistent with our findings [55]. Furthermore, enhanced ferroptosis adds to the antitumor efficacy of immunotherapy [49]. Understanding the role of ferroptosis in immunotherapy has important implications for GC treatment options. Two well-known immunotherapeutic targets are CTLA-4 and PD-L1/PD-1 [55]. We calculated the responsiveness to immunotherapy (CTLA-4 or PD-1 targeted) of the two groups. In the high-risk group, immunotherapy was less effective. This implies that following ferroptosis, cells are more susceptible to immunotherapy. As a result, establishing FRA phenotypes may influence immunotherapy and targeted therapy outcomes. Evaluating patient FRA signatures may provide valuable information for decision-making in prospective tailored treatments.

Several factors, including the strength of the splice site, *cis*-regulatory sequences in pre-mRNAs, and *trans*-acting factor expression levels, influence the relative abundance of AS to produce distinct AS isoforms [15]. Consequently, correlation analysis of SF expression levels and the PSI values of AS events was performed to study the mechanism of FRAs, which could provide more systematic knowledge of the molecular regulatory mechanisms of FRAs in GC. In this study, we screened 15 SF genes through univariate analysis and correlated these 15 genes with 12 model related AS events. Among these genes, SF3A2 had the strongest association with FBXW7 (cor = 0.476). Therefore, we chose to investigate the splicing effect of SF3A2 on FBXW7 in GC cells. However, due to lack of research evidence, we did not consider the effect of SF3A2 on the potential biological behavior of GC under the splicing effect of FBXW7. SF3A2 is a subunit of the SF SF3a, which also includes SF3A1 and SF3A3. SF3a is required for the in vitro synthesis of the functional 17S U2 snRNP and prespliceosome assembly [56]. SF3A1 and SF3A3 have been linked to tumor growth in the previous studies [57–60]. Furthermore, SF3A2 appears to have a more significant relationship in GC. We used siSF3A2 cells to perform assays to assess ROS and total iron ion levels. In siSF3A2 cells treated with erastin, ferroptosis was likewise significantly enhanced. As a result, SF3A2 improved the resistance of GC cells to ferroptosis. Ferroptosis is more common in cells with low SF3A2 expression, inhibiting GC development. SF3A2 may regulate cellular ferroptosis by altering the differential transcripts of a selection of important FRGs. As a result, AS has a significant impact on the biological function of FRGs, and examining machine-processed gene transcripts may help us understand ferroptosis at a deeper level. SF3A2 was also found to be crucial in the proliferation of GC cells. This finding implies that SF3A2 may operate as a proto-oncogene, and more research is needed to focus on SF3A2's mechanistic role in tumor growth and progression.

Finally, in our investigation, we developed FRA-related biomarkers and a therapeutically effective predictive signature to highlight the prognostic usefulness of FRGs and associated AS events in GC. Unlike prior AS analyses, our focus on FRGs may open up new avenues and possibilities for studying ferroptosis mechanisms in GC. However, our study had some limitations. First, discrepancies in PSI values might have arisen due to heterogeneous in GC samples, the PSI values are highly sensitive and can be significantly affected by the methods of RNA extraction and storage, as well as RNA-Seq protocols. Second, while we verified the regulatory role of SF3A2 in FBXW7, we did not find a direct interaction between SF3A2 and FBXW7 pre-mRNA. Furthermore, the specific FRAs that played a major role in GC were not identified, nor was the mechanism by which FRA-induced ferroptosis affects GC elucidated. Overall, our findings provide useful information in the search for effective ferroptosis-based therapy for GC.

5. Conclusion

We discovered predictive AS events for FRGs and used 12 FRAs to build a high-performance prognostic signature. This signature outperformed conventional pathological features in terms of patient prognosis. The association between the risk signature and the immunological landscape was investigated in the preliminary stage. The finding of SF-FRAs contributes to our understanding of the potential mechanisms of ferroptosis. Finally, the AS signature we developed predicts clinical outcomes in GC patients, and the FRA analysis provides references and possibilities for ferroptosis research.

Ethics approval and consent to participate

Not applicable.

Consent for publish

All authors agree to submit for consideration for publication in the journal.

Data availability statement

Data will be made available on request. The bioinformatic data of this study was from the gastric adenocarcinoma cohort of TCGA. RNA expression data, clinical data could be downloaded. (https://portal.gdc.cancer.gov/). Alternative splicing data could be download in https://bioinformatics.mdanderson.org/TCGASpliceSeq/. Ferroptosis-related gene sets can be downloaded in FerrDb (http://www.zhounan.org/ferrdb).

Funding

China Primary Health Care Foundation (2022018).

Authors' contributions

Gang Long and Zhiyong Li analyzed the data, drew the figures, wrote the manuscript, and completed in vitro experiments. Irankunda Eric Daniel polished the article. Yue Gao, Xu Zhang, Xiyang Cheng, Lisha Zhang contributed to the critical revision of the manuscript. Dawei Wang reviewed and edited. Zhengtian Li designed the study, supervised this study, provided Funding, wrote - reviewed and edited.

CRediT authorship contribution statement

Gang Long: Writing – original draft, Visualization, Validation, Software, Methodology, Investigation, Formal analysis, Data curation, Conceptualization. **Zhiyong Li:** Writing – original draft, Visualization, Validation, Software, Methodology, Investigation, Formal analysis, Data curation, Conceptualization. **Yue Gao:** Writing – original draft, Visualization, Supervision. **Xu Zhang:** Writing – original draft, Visualization. **Xiyang Cheng:** Writing – original draft, Visualization. **Irankunda Eric Daniel:** Writing – review & editing, Writing – original draft, Methodology, Investigation. **Lisha Zhang:** Writing – original draft, Visualization. **Dawei Wang:** Writing – review & editing, Supervision. **Zhengtian Li:** Writing – review & editing, Supervision, Funding acquisition, Conceptualization.

Declaration of generative AI and AI-assisted technologies in the writing process

During the preparation of this work, we used Chatgpt4 to polish writing and enhance readability. After using this tool, we reviewed and edited the content as needed and take full responsibility for the content of the publication.

Declaration of competing interest

The authors declare that they have no known competing financial interests or personal relationships that could have appeared to influence the work reported in this paper.

Acknowledgements

Not applicable.

Appendix A. Supplementary data

Supplementary data to this article can be found online at https://doi.org/10.1016/j.heliyon.2024.e34381.

References

[1] R.L. Siegel, K.D. Miller, H.E. Fuchs, A. Jemal, Cancer statistics, 2022, Ca - Cancer J. Clin. 72 (1) (2022) 7–33.
[2] E.C. Smyth, M. Nilsson, H.I. Grabsch, N.C.T. van Grieken, F. Lordick, Gastric cancer, Lancet 396 (10251) (2020) 635–648.
[3] S.S. Joshi, B.D. Badgwell, Current treatment and recent progress in gastric cancer, Ca - Cancer J. Clin. 71 (3) (2021) 264–279.
[4] J. Pan, X. Zhang, X. Fang, Z. Xin, Construction on of a ferroptosis-related lncRNA-based model to improve the prognostic evaluation of gastric cancer patients based on bioinformatics, Front. Genet. 12 (2021).
[5] J. Xiao, L. Zheng, J. Liu, Comprehensive analysis of the aberrance and functional significance of ferroptosis in gastric cancer, Front. Pharmacol. 13 (2022).
[6] S.J. Dixon, K.M. Lemberg, M.R. Lamprecht, R. Skouta, E.M. Zaitsev, C.E. Gleason, D.N. Patel, A.J. Bauer, A.M. Cantley, W.S. Yang, B. Morrison 3rd, B. R. Stockwell, Ferroptosis: an iron-dependent form of nonapoptotic cell death, Cell 149 (5) (2012) 1060–1072.
[7] W.S. Yang, B.R. Stockwell, Ferroptosis: death by lipid peroxidation, Trends Cell Biol. 26 (3) (2016) 165–176.
[8] B.R. Stockwell, X. Jiang, W. Gu, Emerging mechanisms and disease relevance of ferroptosis, Trends Cell Biol. 30 (6) (2020) 478–490.
[9] X. Jiang, B.R. Stockwell, M. Conrad, Ferroptosis: mechanisms, biology and role in disease, Nat. Rev. Mol. Cell Biol. 22 (4) (2021) 266–282.
[10] H. Zhang, T. Deng, R. Liu, T. Ning, H. Yang, D. Liu, Q. Zhang, D. Lin, S. Ge, M. Bai, X. Wang, L. Zhang, H. Li, Y. Yang, Z. Ji, H. Wang, G. Ying, Y. Ba, CAF secreted miR-522 suppresses ferroptosis and promotes acquired chemo-resistance in gastric cancer, Mol. Cancer 19 (1) (2020) 43.
[11] J.Y. Lee, M. Nam, H.Y. Son, K. Hyun, S.Y. Jang, J.W. Kim, M.W. Kim, Y. Jung, E. Jang, S.J. Yoon, J. Kim, J. Kim, J. Seo, J.K. Min, K.J. Oh, B.S. Han, W.K. Kim, K. H. Bae, J. Song, J. Kim, Y.M. Huh, G.S. Hwang, E.W. Lee, S.C. Lee, Polyunsaturated fatty acid biosynthesis pathway determines ferroptosis sensitivity in gastric cancer, Proc. Natl. Acad. Sci. U.S.A. 117 (51) (2020) 32433–32442.
[12] Y. Wang, L. Zheng, W. Shang, Z. Yang, T. Li, F. Liu, W. Shao, L. Lv, L. Chai, L. Qu, Q. Xu, J. Du, X. Liang, J. Zeng, J. Jia, Wnt/beta-catenin signaling confers ferroptosis resistance by targeting GPX4 in gastric cancer, Cell Death Differ 29 (11) (2022) 2190–2202.
[13] B.R. Stockwell, J.P. Friedmann Angeli, H. Bayir, A.I. Bush, M. Conrad, S.J. Dixon, S. Fulda, S. Gascon, S.K. Hatzios, V.E. Kagan, K. Noel, X. Jiang, A. Linkermann, M.E. Murphy, M. Overholtzer, A. Oyagi, G.C. Pagnussat, J. Park, Q. Ran, C.S. Rosenfeld, K. Salnikow, D. Tang, F.M. Torti, S.V. Torti, S. Toyokuni, K.A. Woerpel, D.D. Zhang, Ferroptosis: a regulated cell death nexus linking metabolism, Redox Biology, and Disease, Cell 171 (2) (2017) 273–285.
[14] N. Zhou, J. Bao, FerrDb: a manually curated resource for regulators and markers of ferroptosis and ferroptosis-disease associations, Database 2020 (2020).
[15] F.E. Baralle, J. Giudice, Alternative splicing as a regulator of development and tissue identity, Nat. Rev. Mol. Cell Biol. 18 (7) (2017) 437–451.
[16] Y. Lee, D.C. Rio, Mechanisms and regulation of alternative pre-mRNA splicing, Annu. Rev. Biochem. 84 (2015) 291–323.
[17] J. Ule, B.J. Blencowe, Alternative splicing regulatory networks: functions, mechanisms, and evolution, Mol Cell 76 (2) (2019) 329–345.
[18] M. Montes, B.L. Sanford, D.F. Comiskey, D.S. Chandler, RNA splicing and disease: animal models to therapies, Trends Genet. 35 (1) (2019) 68–87.
[19] L. Frankiw, D. Baltimore, G. Li, Alternative mRNA splicing in cancer immunotherapy, Nat. Rev. Immunol. 19 (11) (2019) 675–687.
[20] S.C. Bonnal, I. Lopez-Oreja, J. Valcarcel, Roles and mechanisms of alternative splicing in cancer - implications for care, Nat. Rev. Clin. Oncol. 17 (8) (2020) 457–474.
[21] A. Kahles, K.V. Lehmann, N.C. Toussaint, M. Huser, S.G. Stark, T. Sachsenberg, O. Stegle, O. Kohlbacher, C. Sander, N. Cancer Genome Atlas Research, G. Ratsch, Comprehensive analysis of alternative splicing across tumors from 8,705 patients, Cancer Cell 34 (2) (2018) 211–224 e6.
[22] X. Wang, J. Li, X. Bian, C. Wu, J. Hua, S. Chang, T. Yu, H. Li, Y. Li, S. Hu, G. Shan, W. Lin, CircURI1 interacts with hnRNPM to inhibit metastasis by modulating alternative splicing in gastric cancer, Proc. Natl. Acad. Sci. U.S.A. 118 (33) (2021).
[23] D. Ray, Y.C. Yun, M. Idris, S. Cheng, A. Boot, T.B.H. Iain, S.G. Rozen, P. Tan, D.M. Epstein, A tumor-associated splice-isoform of MAP2K7 drives dedifferentiation in MBNL1-low cancers via JNK activation, Proc. Natl. Acad. Sci. U.S.A. 117 (28) (2020) 16391–16400.
[24] M. Seiler, S. Peng, A.A. Agrawal, J. Palacino, T. Teng, P. Zhu, P.G. Smith, N. Cancer Genome Atlas Research, S. Buonamici, L. Yu, Somatic mutational landscape of splicing factor genes and their functional consequences across 33 cancer types, Cell Rep. 23 (1) (2018) 282–296 e4.
[25] J.R. Conway, A. Lex, N. Gehlenborg, UpSetR: an R package for the visualization of intersecting sets and their properties, Bioinformatics 33 (18) (2017) 2938–2940.
[26] N. Simon, J. Friedman, T. Hastie, R. Tibshirani, Regularization paths for cox's proportional hazards model via coordinate descent, J. Stat. Software 39 (5) (2011) 1–13.
[27] P. Blanche, J.F. Dartigues, H. Jacqmin-Gadda, Estimating and comparing time-dependent areas under receiver operating characteristic curves for censored event times with competing risks, Stat. Med. 32 (30) (2013) 5381–5397.
[28] Z. Zhang, M.W. Kattan, Drawing Nomograms with R: applications to categorical outcome and survival data, Ann. Transl. Med. 5 (10) (2017) 211.
[29] G. Yu, L.G. Wang, Y. Han, Q.Y. He, clusterProfiler: an R package for comparing biological themes among gene clusters, OMICS 16 (5) (2012) 284–287.
[30] A.M. Newman, C.L. Liu, M.R. Green, A.J. Gentles, W. Feng, Y. Xu, C.D. Hoang, M. Diehn, A.A. Alizadeh, Robust enumeration of cell subsets from tissue expression profiles, Nat. Methods 12 (5) (2015) 453–457.
[31] L. Huang, C. Wu, D. Xu, Y. Cui, J. Tang, Screening of important factors in the early sepsis stage based on the evaluation of ssGSEA algorithm and ceRNA regulatory network, Evol Bioinform Online 17 (2021) 11769343211058463.
[32] K.M. Mahoney, P.D. Rennert, G.J. Freeman, Combination cancer immunotherapy and new immunomodulatory targets, Nat. Rev. Drug Discov. 14 (8) (2015) 561–584.
[33] J.B. Wang, P. Li, X.L. Liu, Q.L. Zheng, Y.B. Ma, Y.J. Zhao, J.W. Xie, J.X. Lin, J. Lu, Q.Y. Chen, L.L. Cao, M. Lin, L.C. Liu, N.Z. Lian, Y.H. Yang, C.M. Huang, C. H. Zheng, An immune checkpoint score system for prognostic evaluation and adjuvant chemotherapy selection in gastric cancer, Nat. Commun. 11 (1) (2020) 6352.
[34] P. Geeleher, N. Cox, R.S. Huang, pRRophetic: an R package for prediction of clinical chemotherapeutic response from tumor gene expression levels, PLoS One 9 (9) (2014) e107468.
[35] P. Jiang, S. Gu, D. Pan, J. Fu, A. Sahu, X. Hu, Z. Li, N. Traugh, X. Bu, B. Li, J. Liu, G.J. Freeman, M.A. Brown, K.W. Wucherpfennig, X.S. Liu, Signatures of T cell dysfunction and exclusion predict cancer immunotherapy response, Nat. Med. 24 (10) (2018) 1550–1558.
[36] S. Hao, J. Yu, W. He, Q. Huang, Y. Zhao, B. Liang, S. Zhang, Z. Wen, S. Dong, J. Rao, W. Liao, M. Shi, Cysteine dioxygenase 1 mediates erastin-induced ferroptosis in human gastric cancer cells, Neoplasia 19 (12) (2017) 1022–1032.
[37] Z. Lin, J. Song, Y. Gao, S. Huang, R. Dou, P. Zhong, G. Huang, L. Han, J. Zheng, X. Zhang, S. Wang, B. Xiong, Hypoxia-induced HIF-1alpha/lncRNA-PMAN inhibits ferroptosis by promoting the cytoplasmic translocation of ELAVL1 in peritoneal dissemination from gastric cancer, Redox Biol. 52 (2022) 102312.
[38] Y. Su, B. Zhao, L. Zhou, Z. Zhang, Y. Shen, H. Lv, L.H.H. AlQudsy, P. Shang, Ferroptosis, a novel pharmacological mechanism of anti-cancer drugs, Cancer Lett. 483 (2020) 127–136.
[39] C. Viallard, B. Larrivee, Tumor angiogenesis and vascular normalization: alternative therapeutic targets, Angiogenesis 20 (4) (2017) 409–426.
[40] A. Kirtonia, G. Sethi, M. Garg, The multifaceted role of reactive oxygen species in tumorigenesis, Cell. Mol. Life Sci. 77 (22) (2020) 4459–4483.
[41] G. Hoxhaj, B.D. Manning, The PI3K-AKT network at the interface of oncogenic signalling and cancer metabolism, Nat. Rev. Cancer 20 (2) (2020) 74–88.
[42] A.A. Belaidi, S. Masaldan, A. Southon, P. Kalinowski, K. Acevedo, A.T. Appukuttan, S. Portbury, P. Lei, P. Agarwal, S.E. Leurgans, J. Schneider, M. Conrad, A. I. Bush, S. Ayton, Apolipoprotein E potently inhibits ferroptosis by blocking ferritinophagy, Mol. Psychiatr. 29 (2) (2024) 211–220.
[43] S. Pal, R. Gupta, R.V. Davuluri, Alternative transcription and alternative splicing in cancer, Pharmacol. Ther. 136 (3) (2012) 283–294.
[44] H. Laubli, L. Borsig, Altered cell adhesion and glycosylation promote cancer immune suppression and metastasis, Front. Immunol. 10 (2019) 2120.
[45] S. Shah, E.J. Brock, K. Ji, R.R. Mattingly, Ras and Rap1: a tale of two GTPases, Semin. Cancer Biol. 54 (2019) 29–39.
[46] N.A. Espinoza-Sanchez, M. Gotte, Role of cell surface proteoglycans in cancer immunotherapy, Semin. Cancer Biol. 62 (2020) 48–67.
[47] J. Liu, S. Zhu, L. Zeng, J. Li, D.J. Klionsky, G. Kroemer, J. Jiang, D. Tang, R. Kang, DCN released from ferroptotic cells ignites AGER-dependent immune responses, Autophagy 18 (9) (2022) 2036–2049.
[48] H. Xu, D. Ye, M. Ren, H. Zhang, F. Bi, Ferroptosis in the tumor microenvironment: perspectives for immunotherapy, Trends Mol. Med. 27 (9) (2021) 856–867.

[49] R. Tang, J. Xu, B. Zhang, J. Liu, C. Liang, J. Hua, Q. Meng, X. Yu, S. Shi, Ferroptosis, necroptosis, and pyroptosis in anticancer immunity, J. Hematol. Oncol. 13 (1) (2020) 110.
[50] C. Xu, S. Sun, T. Johnson, R. Qi, S. Zhang, J. Zhang, K. Yang, The glutathione peroxidase Gpx4 prevents lipid peroxidation and ferroptosis to sustain Treg cell activation and suppression of antitumor immunity, Cell Rep. 35 (11) (2021) 109235.
[51] <46 AN im.pdf>.
[52] Y. Yang, Y. Wang, L. Guo, W. Gao, T.L. Tang, M. Yan, Interaction between macrophages and ferroptosis, Cell Death Dis. 13 (4) (2022) 355.
[53] E. Dai, L. Han, J. Liu, Y. Xie, G. Kroemer, D.J. Klionsky, H.J. Zeh, R. Kang, J. Wang, D. Tang, Autophagy-dependent ferroptosis drives tumor-associated macrophage polarization via release and uptake of oncogenic KRAS protein, Autophagy 16 (11) (2020) 2069–2083.
[54] C. Liang, X. Zhang, M. Yang, X. Dong, Recent progress in ferroptosis inducers for cancer therapy, Adv. Mater. 31 (51) (2019) e1904197.
[55] D.S. Chen, I. Mellman, Elements of cancer immunity and the cancer-immune set point, Nature 541 (7637) (2017) 321–330.
[56] G. Tanackovic, A. Kramer, Human splicing factor SF3a, but not SF1, is essential for pre-mRNA splicing in vivo, Mol. Biol. Cell 16 (3) (2005) 1366–1377.
[57] 61 Sf3a1 and Pancreatic Cancer New Evi Source Oncotarget So 2015 Oct 15.Pdf>.
[58] C.A. Larsson, G. Cote, A. Quintas-Cardama, The changing mutational landscape of acute myeloid leukemia and myelodysplastic syndrome, Mol. Cancer Res. 11 (8) (2013) 815–827.
[59] M. Ciesla, P.C.T. Ngoc, E. Cordero, A.S. Martinez, M. Morsing, S. Muthukumar, G. Beneventi, M. Madej, R. Munita, T. Jonsson, K. Lovgren, A. Ebbesson, B. Nodin, I. Hedenfalk, K. Jirstrom, J. Vallon-Christersson, G. Honeth, J. Staaf, D. Incarnato, K. Pietras, A. Bosch, C. Bellodi, Oncogenic translation directs spliceosome dynamics revealing an integral role for SF3A3 in breast cancer, Mol Cell 81 (7) (2021) 1453–1468 e12.
[60] D. Chen, H. Zhou, Z. Cai, K. Cai, J. Liu, W. Wang, H. Miao, H. Li, R. Li, X. Li, Y. Chen, H.Y. Wang, Z. Wen, CircSCAP interacts with SF3A3 to inhibit the malignance of non-small cell lung cancer by activating p53 signaling, J. Exp. Clin. Cancer Res. 41 (1) (2022) 120.